

# Single Crystal Study of Competing Rhombohedral and Monoclinic Order in Lead Zirconate Titanate

D. Phelan<sup>1</sup>, X. Long<sup>2</sup>, Y. Xie<sup>2</sup>, Z.-G. Ye<sup>2</sup>, A. M. Glazer<sup>3</sup>, H. Yokota<sup>4</sup>, P. A. Thomas<sup>5</sup>, P. M. Gehring<sup>1</sup>

<sup>1</sup>*NIST Center for Neutron Research,  
National Institute of Standards and Technology,  
Gaithersburg, Maryland 20899, USA*

<sup>2</sup>*Department of Chemistry, Simon Fraser University,  
Burnaby, BC, V5A 1S6, Canada*

<sup>3</sup>*Clarendon Laboratory, Department of Physics,  
University of Oxford, Parks Road,  
Oxford OX1 3PU, United Kingdom*

<sup>4</sup>*Department of Bioengineering,  
University of Tokyo, Tokyo 113-8656, Japan*

<sup>5</sup>*Department of Physics, University of Warwick,  
Coventry CV4 7AL, United Kingdom*

Neutron diffraction data obtained on single crystals of  $\text{PbZr}_{1-x}\text{Ti}_x\text{O}_3$  with  $x = 0.325$  and  $x = 0.460$ , which lie on the pseudorhombohedral side of the morphotropic phase boundary, suggest a coexistence of rhombohedral ( $R3m/R3c$ ) and monoclinic ( $Cm$ ) domains and that monoclinic order is enhanced by Ti substitution. A monoclinic phase with a doubled unit cell ( $Cc$ ) is ruled out as the ground state.

A hallmark of highly piezoelectric perovskite materials, such as  $\text{PbZr}_{1-x}\text{Ti}_x\text{O}_3$  (PZT), is a morphotropic phase boundary (MPB) that segregates two compositional regimes into different ferroelectric states and pinpoints the range of substitutions for which the piezoelectric response is optimal. For PZT (and other Pb-based materials), the MPB ostensibly divides regions of Ti-poor rhombohedral ( $R3m$ ) and Ti-rich tetragonal ( $P4mm$ ) order. The discovery of an intermediate monoclinic phase within a narrow compositional range near the MPB [1,2] provided a mechanism whereby PZT could transform from  $R3m$  to  $P4mm$  via a common subgroup,  $Cm$ . This led to the idea that enhanced piezoelectricity at the MPB arises from the freedom of the Pb atom to move within the mirror plane of the monoclinic phase, thus allowing the electric polarization to rotate [3,4]. Alternatively, the adaptive-phases model, proposes that the lower symmetry allows for complex domain structures in which the net polarization can be made to change direction via domain populations [5]. These mechanisms remain controversial as how the phase symmetry is transformed across the phase diagram remains unclarified.

The most recent measurements identify no clear phase boundary between rhombohedral and monoclinic phases [6]. Instead the anisotropic Pb displacement ellipsoid is highly flattened perpendicular to the polar displacement direction, which led to the suggestion that some kind of disorder [7,8] or local monoclinic displacements [9] are present in the rhombohedral phases. From this followed the idea that the local symmetries are monoclinic, but that the coherence lengths are limited to just a few unit cells so that diffraction methods yield only rhombohedral symmetries for Ti-poor compositions [10].

While this model is able to explain the lack of an R-M phase boundary, two different explanations were recently put forth. The first, based on refinements of synchrotron data, replaces the rhombohedral phases with a high-temperature monoclinic  $Cm$  and a low-temperature monoclinic  $Cc$  phase (the  $Cc$  phase superimposes antiferrodistortive displacements with the ferroelectric displacements of  $Cm$ , causing the unit cell to double as depicted in Ref. [11]) [11,12]. The second, based on a separate set of neutron diffraction refinements favors a coexistence of rhombohedral  $R3c$  and monoclinic  $Cm$  (but not  $Cc$ ) phases at room temperature in the Ti-poor region [6]. The present results resolve this issue conclusively.

A hindrance to precise symmetry determination of PZT has been the difficulty to grow single crystals. Therefore, structural studies near the MPB have been limited to powders and ceramics. A major problem with Rietveld refinement of highly pseudosymmetric polycrystalline materials is that many models refine to similar agreement factors, which makes it nearly impossible to choose between them. Very recently, single crystals were grown at Simon Fraser University using a top-seeded solution growth technique. The crystals measured here have compositions of  $x = 0.325$  (dimensions  $3.3 \text{ mm} \times 2.1 \text{ mm} \times 1.1 \text{ mm}$ ) and  $x = 0.460$  ( $3.0 \text{ mm} \times 2.7 \text{ mm} \times 0.6 \text{ mm}$ ). The measurements were performed at the NIST Center for Neutron Research (NCNR) on thermal (BT-9) and cold (SPINS) triple-axis spectrometers. Various instrumental configurations were employed and are given in the figure captions. The samples were measured under vacuum in a closed-cycle helium refrigerator. Miller indices are expressed with respect to the aristotype cubic cell with a lattice parameter  $a \approx 4.1 \text{ \AA}$ .

Structural transitions in each crystal were characterized by measurements of the 200 Bragg reflection as a function of temperature (see Fig. 1). For  $x = 0.325$ , two phase transitions were identified corresponding to paraelectric-ferroelectric and ferroelectric-ferroelectric transitions. One occurs near 370 K and is marked by a change in the slope of the temperature dependence of the rocking curve width, a strong shift in the peak position of the rocking scan, and a change from positive to negative volume thermal expansion. A second near 590 K is evident from the large change in intensity resulting from a release of secondary extinction, a leveling out of the width of the rocking curve, and a return to positive volume thermal expansion. Similar measurements for  $x = 0.460$  revealed more complicated behavior. Possible phase transitions are seen at 220, 410, 480, 540, and 650 K. Between 480 and 540 K the volume thermal expansion is  $\approx 9.1 \times 10^{-5}$  1/K, or roughly 1 order of magnitude larger than normally observed in oxides; above 540 K a steep negative volume thermal expansion ( $\approx -4.9 \times 10^{-5}$  1/K) is observed. A huge release of extinction occurs upon cooling below the cubic phase. The large number of anomalies is consistent with the fact that the crystal has a composition very close to the MPB. A similarly complex series of phase transitions has been suggested [13] based on powder neutron data [14].

One approach to identify the structural symmetry is to look for superlattice peaks that appear when the primitive unit cell is doubled. The  $R3c$  phase generates superlattice reflections that result from correlated rotations of the oxygen octahedra, but only at the  $R_2$  points  $\frac{h}{2}\frac{k}{2}\frac{k}{2}$ , where  $h$  and  $k$  are odd and  $h \neq k$  (for twinned crystals,  $\frac{h}{2}\frac{k}{2}\frac{k}{2}$  and  $\frac{h}{2}\frac{k}{2}\frac{h}{2}$  are not distinct). This is the only type of superlattice peak that has been observed in x-ray and neutron powder diffraction measurements [6,15,16]. Other superlattice reflections have been observed using electron diffraction methods [15,17-20]; however, these have been argued to result from surface effects or local inhomogeneities, with only  $R_2$  attributed to the bulk [15]. On the other hand, a phase with  $Cc$  symmetry [11,12] would generate weak superlattice reflections at the  $R_1$  points  $\frac{h}{2}\frac{h}{2}\frac{h}{2}$ , where  $h$  is odd. We looked for superlattice reflections in the  $x = 0.325$  crystal in the  $(hk0)$  and  $(hkk)$  scattering planes at 35 K (see Fig. 2). No peaks were found at the  $X$  points  $\frac{1}{2}00$  and  $\frac{3}{2}00$ , or at the  $M$  points  $\frac{1}{2}\frac{1}{2}0$  and  $\frac{3}{2}\frac{3}{2}0$ , however, several  $R_2$  peaks were observed. The order parameter measurement shown in Fig. 2(f) indicates that the  $R_2$  peaks vanish at the low-temperature phase transition identified in Fig. 1(a) ( $\approx 370$  K). Weaker  $R_2$  peaks were observed in the  $x = 0.460$  crystal that vanish above the lowest transition temperature identified in Fig. 1(b) ( $\approx 220$  K). We also observed superlattice peaks at the  $R_1$  points  $\frac{1}{2}\frac{1}{2}\frac{1}{2}$  and  $\frac{3}{2}\frac{3}{2}\frac{3}{2}$ , which showed temperature dependences similar to those of the  $R_2$  points. Because these peaks could be caused by double scattering

as for  $\text{SrTiO}_3$  [21], we performed a standard test in which the peak intensity was measured as a function of the neutron wavelength. Figure 2(e) shows measurements performed with cold neutrons at two different wavelengths. A very strong  $R_1$  peak was observed at  $\frac{1}{2}\frac{1}{2}\frac{1}{2}$  when  $\lambda = 4.045$  Å; however, when the wavelength was increased to 5.222 Å, so that all  $R_2$  reflections fell outside the Ewald sphere, this  $R_1$  peak completely disappeared. Hence, we can definitively conclude that the observed  $R_1$  peak results from double scattering. We have determined with 99% statistical confidence that the maximum ratio of the peak intensity  $\frac{1}{2}\frac{1}{2}\frac{1}{2}$  compared with that of 100 is 0.002% ( $x = 0.325$ ) and 0.003% ( $x = 0.460$ ). These are extremely severe limits: for the refinement listed in Ref. [22], which is for a sample with  $x = 0.48$  at 10 K, the calculated intensity ratio is 0.13% (nearly 40 times larger than our limit for  $x = 0.46$ ), while refinement for a sample with  $x = 0.30$  at 300 K [23] gives a ratio of 3.8% (more than 1000 times larger). Therefore, our superlattice survey is consistent with an  $R3c$  ground state and effectively rules out the presence of any phase, such as  $Cc$  or even triclinic symmetry, that would generate  $R_1$  superlattice peaks for either sample.

Symmetries were further studied by high resolution radial measurements of several Bragg reflections, which is possible because the crystals are multidomain. The 200 reflection can be used to distinguish between  $Cm$  and  $R3m/R3c$  phases because it splits into a doublet under  $Cm$  but remains a singlet for  $R3m/R3c$ . We achieved extraordinary wave-vector resolution for this peak by employing a perfect single crystal of Ge as analyzer and exploiting the fact that the Ge 220 reflection spacing almost exactly matches that of the PZT 200 Bragg peak. A peculiarity of this special setup is that the radial linewidth becomes coupled to the sample mosaicity [24], particularly in the regime where the mosaic spread is less than  $20'$ . As shown in Fig. 3(a), a narrow radial linewidth was observed at 200 in the cubic phase (640 K) for  $x = 0.325$  that is nonetheless significantly broader than that measured on a single crystal of  $\text{SrTiO}_3$ . The extra linewidth is well accounted for by the small, but non-negligible mosaic width of the  $x = 0.325$  PZT crystal ( $11'$ ) that was measured under the same conditions in a rocking scan, and which is taken into account in the resolution calculation. From Fig. 1(a) we know that the mosaic width increases as the temperature is lowered; thus the 200 radial linewidth will necessarily broaden as the temperature decreases. Indeed, the 200 radial linewidth at 450K is 12% broader than that at 640 K, but this agrees almost perfectly with the resolution calculation for the broadened mosaic width; hence the radial linewidth of 200 at 450 K is consistent with a resolution-limited peak as would be expected for  $R3m$ . However, at 40 K the peak has broadened by an additional 10% from its value at 450 K, while our resolution calculation predicts a change of only 2%. Given the larger intrinsic mosaic

width of the  $x = 0.460$  its 200 reflection was measured using very tight beam collimations and a conventional PG analyzer, for which the resolution is essentially decoupled from the mosaic width. These data, shown in Fig. 3(b), reveal a broadening of 200 as the temperature is lowered that is even larger than that for  $x = 0.325$ .

The broadened 200 Bragg peaks could result from microscopic strain, finite domain sizes, or a very small  $Cm$  distortion [6]. Microscopic strain and unresolved monoclinic distortions have the same  $Q$  dependence and are impossible to distinguish in our measurements. However, the intrinsically broad 200 linewidths are consistent with recent neutron powder diffraction studies that indicate that the best refinements are obtained with a model of coexisting  $R3c$  and  $Cm$  phases [6]. It is difficult to extract quantitative information about the  $Cm$  phase because the 200 Bragg peak is only slightly broader than the instrumental resolution and can be fit in many different ways. However, we can extract important information about the  $R3c$  phase because it generates a superlattice peak that depends only on the rhombohedral structural correlations. To this end we measured radial scans through the  $R_2$  superlattice peak for both compositions with tight beam collimations at low temperature, as shown in Fig. 4. The two crystals exhibit markedly different linewidths: the peak for  $x = 0.325$  is narrow and close to the resolution limit whereas that for  $x = 0.460$  is severely broadened. A superposition of two resolution-limited Gaussians cannot reproduce this broadening. Instead, the broadening implies the presence of either finite regions of correlated octahedral rotations or microstrain. Generally, there is no microstrain associated with oxygen octahedral rotations. Thus, the most likely explanation for the change in linewidth is that the coherence length of the rotations is diminished. This is an intriguing result, especially when considered in conjunction with the broadened 200 Bragg peaks, because it suggests that the structural correlations in PZT gradually evolve with Ti content from being predominantly long-range rhombohedral for compositions far from the MPB to being predominantly long-range monoclinic for compositions close to the MPB.

The radial line shapes of 200, the appearance of superlattice peaks at  $R_2$  points at low temperature, and the absence of superlattice peaks at  $R_1$  points are consistent with a purely  $R3m$  high-temperature ferroelectric phase for  $x = 0.325$  and coexisting ( $R3m$ ) and ( $Cm$ ) phases for  $x = 0.460$ , and coexisting  $R3c$  and  $Cm$  ground-state ferroelectric phases for both compositions. In addition, the marked broadening of the superlattice peak at  $\frac{3}{2}\frac{1}{2}\frac{1}{2}$ , which is generated by  $R3c$  symmetry, suggests a scenario of competing rhombohedral and monoclinic order in highly piezoelectric compositions in which the rhombohedral correlations become increasingly short-range upon approaching the MPB. This picture lends support to the recent theoretical ideas that the tendency to form

macroscopic monoclinic phases facilitates the mechanism of polarization rotation [25], achieved either by having the freedom to change the direction of Pb displacements within monoclinic unit cells or through the change in the population of twinned monoclinic components under an applied stress or electric field. The elucidation of the correct symmetries of PZT close to the MPB is critical to the theory of the origin of the high piezoelectricity in this and other materials, since it affects the discussion of the numbers and types of microdomains expected as well as the microscopic mechanisms for polarization rotation.

A. M. G. and P. A. T. are grateful for funding from the Engineering and Physical Sciences Research Council (EPSRC) and from the National Science Foundation (NSF). X. L., Y. X., and Z.-G.Y. acknowledge support from the U.S. Office of Naval Research (Grant No. N00014-06-1-0166). This work utilized facilities supported in part by the NSF under Agreement No. DMR-0944772.

- 
- [1] B. Noheda, D. E. Cox, G. Shirane, R. Guo, B. Jones, and L. E. Cross, Phys. Rev. B **63**, 014103 (2000).
  - [2] B. Noheda, D. E. Cox, G. Shirane, J. A. Gonzalo, L. E. Cross, and S. E. Park, Appl. Phys. Lett. **74**, 2059 (1999).
  - [3] L. Bellaiche, A. Garcia, and D. Vanderbilt, Phys. Rev. Lett. **84**, 5427 (2000).
  - [4] H. Fu and R. E. Cohen, Nature (London) **403**, 281 (2000).
  - [5] Y. M. Jin, Y. U. Wang, A. G. Khachatryan, J. Li, and D. Viehland, J. Appl. Phys. **94**, 3629 (2003).
  - [6] H. Yokota, N. Zhang, A. E. Taylor, P. A. Thomas, and A. M. Glazer, Phys. Rev. B **80**, 104109 (2009).
  - [7] S. A. Mabud, J. Appl. Crystallogr. **13**, 211 (1980).
  - [8] A. M. Glazer, S. A. Mabud, and R. Clarke, Acta Cryst. B **34**, 1060 (1978).
  - [9] D. L. Corker, A. M. Glazer, R. W. Whatmore, A. Stallard, and F. Fauth, J. Phys. Condens. Matter **10**, 6251 (1998).
  - [10] A. M. Glazer, P. A. Thomas, K. Z. Baba-Kishi, G. K. H. Pang, and C. W. Tai, Phys. Rev. B **70**, 184123 (2004).
  - [11] D. Pandey, A. K. Singh, and S. Baik, Acta Crystallogr. Sect. A **64**, 192 (2008).
  - [12] D. M. Hatch, H. T. Stokes, R. Ranjan, Ragini, S. K. Mishra, D. Pandey, and B. J. Kennedy, Phys. Rev. B **65**, 212101 (2002).
  - [13] J. Frantii, J. Phys. Chem. B **112**, 6521 (2008).
  - [14] J. Frantii, S. Eriksson, S. Hull, V. Lantto, H. Rundlof, and M. Kakihana, J. Phys. Condens. Matter **15**, 6031 (2003).
  - [15] J. Ricote, D. L. Corker, R. W. Whatmore, S. A. Impey, A. M. Glazer, J. Dec, and K. Roleder, J. Phys. Condens. Matter **10**, 1767 (1998).
  - [16] D. Pandey and Ragini, Z. Kristallogr. **218**, 1 (2003).
  - [17] D. Viehland, Phys. Rev. B **52**, 778 (1995).
  - [18] X. Dai, Z. Xu, and D. Viehland, J. Am. Ceram. Soc. **78**, 2815 (1995).
  - [19] B. Noheda, L. Wu, and Y. Zhu, Phys. Rev. B **66**, 060103 (2002).

- [20] Ragini, S. K. Mishra, D. Pandey, H. Lemmens, and G. Van Tendeloo, Phys. Rev. B **64**, 054101 (2001).
- [21] G. Shirane, S. M. Shapiro, and J. M. Tranquada, *Neutron scattering with a triple-axis spectrometer* (Cambridge University Press, Cambridge, England, 2002).
- [22] R. Ranjan, A. K. Singh, Ragini, and D. Pandey, Phys. Rev. B **71**, 092101 (2005).
- [23] D. Pandey, Private Communication.
- [24] G. Xu, P. M. Gehring, V. J. Ghosh, and G. Shirane, Acta Crystallogr. Sect. A **60**, 598 (2004).
- [25] A. J. Bell, J. Mater. Sci. **41**, 13 (2006).

### Figure Captions:

#### Fig. 1:

Temperature dependence of the 200 Bragg reflection for (a)  $x = 0.325$  and (b)  $x = 0.460$ . Shown are the integrated intensity, full-width-at-half-maximum (FWHM), and peak position ( $\omega_s$ ) of Gaussian fits to rocking (transverse) scans through the Bragg peak. Also shown is the average unit cell volume (aristotype) determined from Gaussian fits to radial scans through the Bragg peak. Apparent phase transition temperatures are marked by dashed lines. Error bars correspond to uncertainties of  $1\sigma$  in the fitted parameters. Measurements were performed on BT-9 with horizontal beam collimations of  $40^\circ$ - $47^\circ$ - $40^\circ$ - $80^\circ$  and a single PG filter.

#### Fig. 2:

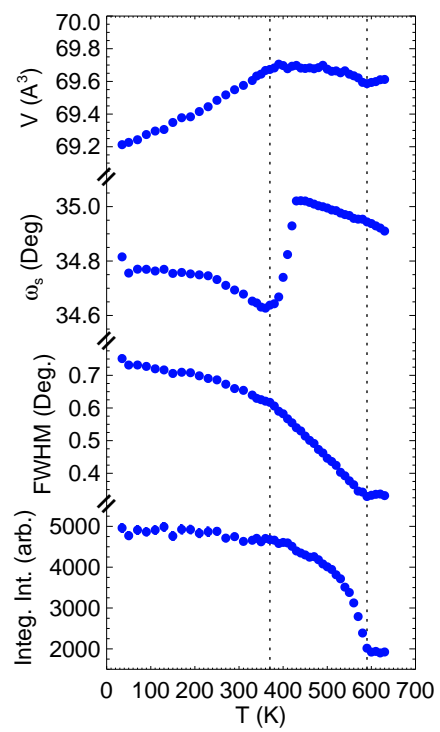
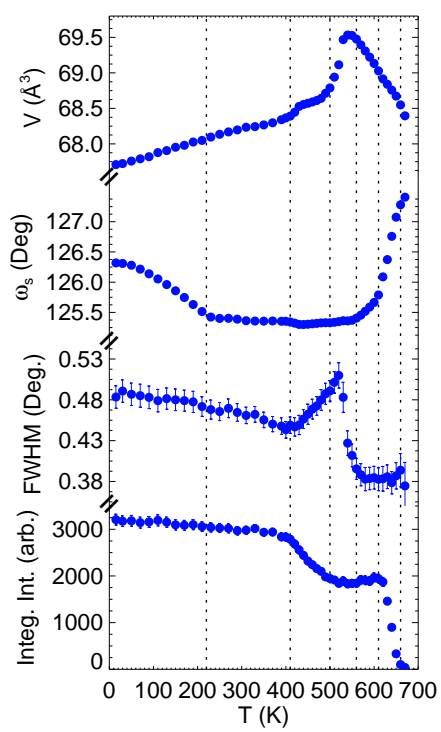
(a)-(c) Radial scans through the  $X$ ,  $M_1$ , and  $M_2$  points reveal no superlattice reflections for  $x = 0.325$  at 35 K. (d) Scans through one  $R_2$  point at various temperatures for  $x = 0.325$ . (e) Scans performed using two wavelengths through an  $R_1$  point for  $x = 0.325$ . (f) The order parameters of the superlattice phases are given by the peak intensity of the  $\frac{5}{2}\frac{1}{2}\frac{1}{2}$  reflection. Error bars represent an uncertainty of  $1\sigma$  in the measured intensities. Scans in (a)-(d) and (f) were made using collimations of  $40^\circ$ - $47^\circ$ - $40^\circ$ - $80^\circ$ , 3 PG filters, and  $\lambda = 2.359$  Å on BT-9. The scans in (e) were made on SPINS with collimations of  $80^\circ$ - $80^\circ$  and two Be filters.

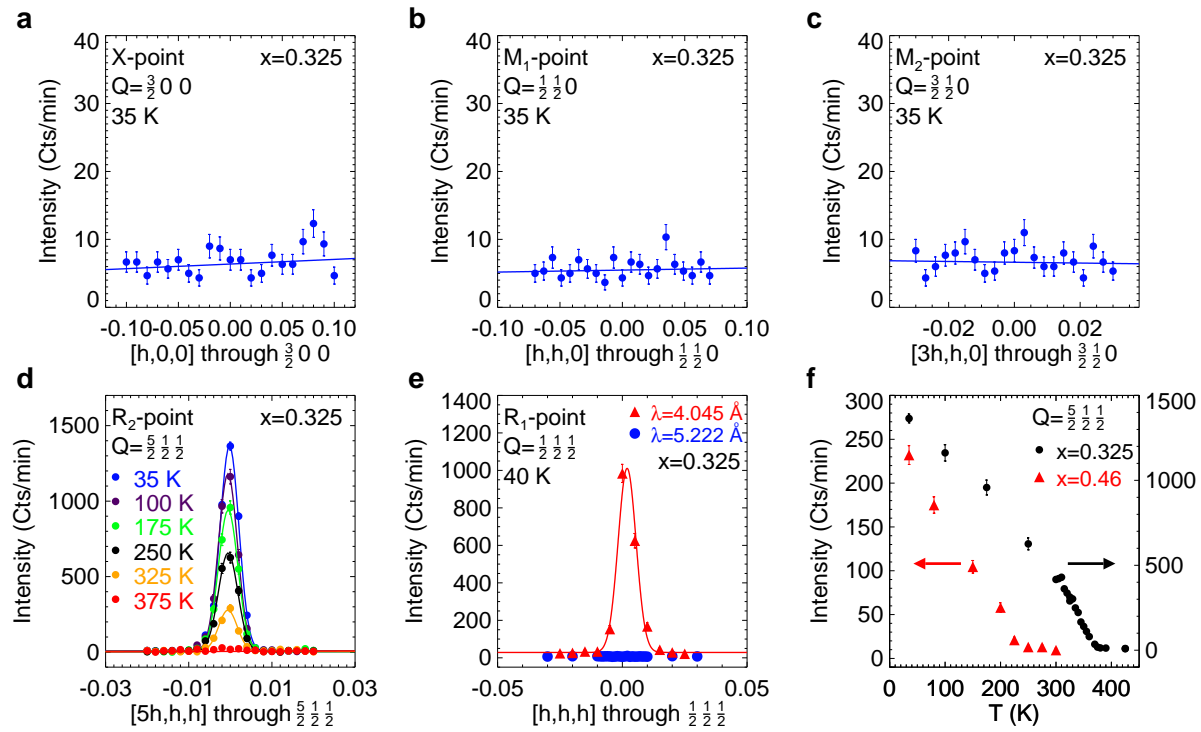
#### Fig. 3:

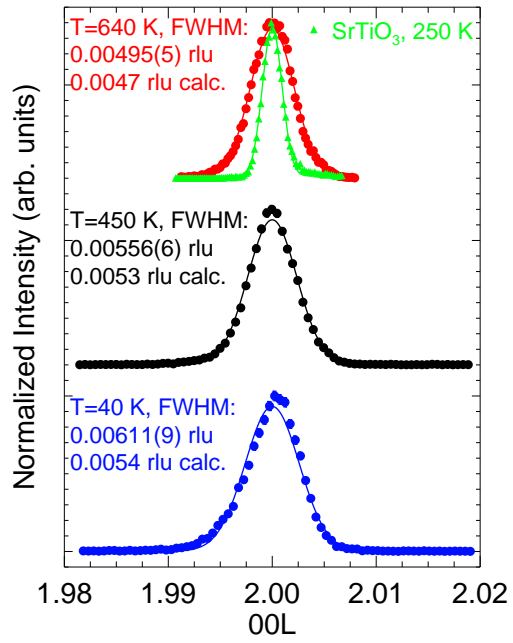
(a) Radial scans through the 200 Bragg reflection of the  $x = 0.325$  crystal at selected temperatures. The measurements were performed on BT-9 with  $\lambda = 2.359$  Å, collimations of  $15^\circ$ - $47^\circ$ - $10^\circ$ - $20^\circ$ , a single PG filter, and the Ge 220 analyzer. Also shown is a measurement of single crystal  $\text{SrTiO}_3$  (data from Ref. [24] represented by green triangles) obtained with collimations of  $10^\circ$ - $40^\circ$ - $20^\circ$ - $40^\circ$ . (b) Radial scans through 200 for the  $x = 0.460$  crystal using the PG 002 analyzer, 3 PG filters, and collimations of  $15^\circ$ - $10^\circ$ - $10^\circ$ - $10^\circ$ .

#### Fig. 4:

High resolution radial scans performed through the  $R_2$  point on SPINS using collimations of G ( $39^\circ$ )- $40^\circ$ - $10^\circ$ - $20^\circ$ , two Be filters, and with  $\lambda = 4.045$  Å.

**a**  $x=0.325$ , 200 Reflection**b**  $x=0.460$ , 200 Reflection



**a** **x=0.325, Ge(220) Analyzer****b** **x=0.460, PG(002) Analyzer**